Biosensors and Bioelectronics 26 (2010) 1337–1345

Contents lists available at ScienceDirect

Biosensors and Bioelectronics

journal homepage: www.elsevier.com/locate/bios

Protein immobilisation on micro/nanostructures fabricated by laser microablation

Dan V. Nicolau [a,b,*], Elena P. Ivanova [b], Florin Fulga [a,b], Luisa Filipponi [b], Andrea Viezzoli [b], Serban Dobroiu [a], Yulia V. Alekseeva [b], Duy K. Pham [b]

[a] Department of Electrical Engineering and Electronics, The University of Liverpool, Brownlow Hill, L69 3GJ, UK
[b] Industrial Research Institute Swinburne, Swinburne University of Technology, PO Box 218, Hawthorn, Vic. 3122, Australia

ARTICLE INFO

Article history:
Received 26 April 2010
Received in revised form 29 June 2010
Accepted 13 July 2010
Available online 17 July 2010

Keywords:
Microarrays
Protein arrays
Protein adsorption
Microablation

ABSTRACT

The performance of biomedical microdevices requires the accurate control of the biomolecule concentration on the surface, as well as the preservation of their bioactivity. This desideratum is even more critical for proteins, which present a significant propensity for surface-induced denaturation, and for microarrays, which require high multiplexing. We have previously proposed a method for protein immobilisation on micro/nanostructures fabricated via laser ablation of a thin metal layer deposited on a transparent polymer. This study investigates the relationship between the properties of the micro/nanostructured surface, i.e., topography and physico-chemistry, and protein immobilisation, for five, molecularly different proteins, i.e., lysozyme, myoglobin, α-chymotrypsin, human serum albumin, and human immunoglobulin. Protein immobilisation on microstructures has been characterised using quantitative fluorescence measurements and atomic force microscopy. It has been found that the sub-micrometer-level, combinatorial nature of the microstructure translates in a 3–10-fold amplification of protein adsorption, as compared to flat, chemically homogenous polymeric surfaces. This amplification is more pronounced for smaller proteins, as they can capitalize better on the newly created surface and variability of the nano-environments.

1. Introduction

While protein based microdevices have already a long tradition, as attractive analytical methods allowing rapid, efficient, and quantitative detection (Chovan and Guttman, 2002; Hook et al., 2010; Ray et al., 2010), the emergence of proteomics made protein microarrays critical tools in diagnostics and drug discovery. Compared with the classical, single-protein-based devices, the new, multiplexed protein micro- and nano-devices pose important technological challenges, mainly arising from (i) the large variety of proteins needed to be immobilised on the same chip surface; (ii) increased density of patterned areas, e.g., spots, immobilising specific proteins as required by high-throughput analysis; and (iii) the ever present complexities of protein–surface interactions, reflecting in complex fabrication and operation. For all these reasons, the simple extrapolation of DNA microarray technology, although attractive, is unwarranted or at least questionable (Hanson et al., 2005).

Most architectures of biomedical microdevices assume that molecularly different biomolecules are immobilised and confined on laterally defined, either flat or profiled micro-areas on the surface of the biochips. Micro- and nano-fabrication techniques developed for semiconductor device manufacturing deliver extreme resolution and repetitive patterning, but require specific materials; can provide only small patterned areas; and require high cost of ownership. As resolution and repetitive patterning are less important; and all other characteristics of semiconductor manufacturing are major roadblocks in the development of biomedical microdevices, new patterning technologies need to be developed. In this context, laser microablation can produce patterns ranging from several tens of microns to few hundreds of nanometres, in virtually any non-transparent material (Steen, 1998), and on large areas.

We described previously (Dobroiu et al., 2010; Ivanova et al., 2002) a method for the fabrication of protein arrays via the immobilisation of proteins on micro/nanostructures fabricated by laser microablation of a thin metal layer deposited on a transparent polymeric substrate. This study uses this system to investigate the interaction between proteins and nanostructures

* Corresponding author at: Department of Electrical Engineering & Electronics, Brownlow Hill, Liverpool, Merseyside L69 3GJ, United Kingdom.
Tel.: +44 0 151 794 4537.
E-mail address: d.nicolau@liverpool.ac.uk (D.V. Nicolau).

0956-5663/$ – see front matter © 2010 Elsevier B.V. All rights reserved.
doi:10.1016/j.bios.2010.07.044

for the benefit of highly sensitive, highly multiplexable protein arrays.

2. Materials and methods

2.1. Fabrication of the microstructures

The procedure for the fabrication of micro/nanostructures, described before (Dobroiu et al., 2010; Ivanova et al., 2002), consist of the following steps. Glass slides or cover slips were thoroughly cleaned, primed with hexamethyldisilazane via spin coating, then spin-coated at 3000 rpm with a 4 wt.% solution of poly(methyl methacrylate) – PMMA – in propylene glycol methyl ether acetate. The coated substrates were then soft baked at 85 °C for 30 min, and stored in a desiccator prior to and after gold deposition. Gold layers of 50 nm thickness have been obtained via the deposition in a sputtering SEM-coating unit E5100 (Polaron Equipment Ltd) at 25 mA for 90 s at 0.1 Torr. The gold-layered substrata were then incubated with bovine serum albumin (BSA) by immersion in a 1% (w/v) BSA 10 mM phosphate-buffered saline (PBS) solution (pH 7.4) at room temperature for approximately 1 h, and then rinsed with PBS followed by Nanopure water.

For the microfabrication step we used a Laser Scissors-Tweezers System, from Cell Robotics, (Albuquerque, NM, USA), mounted on a Nikon inverted microscope (Nikon Eclipse TE-300). The microablation experiments were performed by the pulsed-laser of the Scissors module, which operates at a wavelength 337 nm; used either in single or repetitive mode, with individual pulses lasting 4 ns. While each pulse can deliver up to 220 μJ, we operated at 50% power, i.e., 100 μJ, with an objective of 100× magnification.

2.2. Protein immobilisation on microstructures

Lysozyme, myoglobin, α-chymotrypsin, human serum albumin (HSA) and human immunoglobulin (IgG), were purchased from Sigma. The proteins were prepared as stock solutions at a concentration of 2 mg/ml and diluted with TBS to 100 μg/ml as working solutions prior to experiments.

AlexaFluor 546 has been conjugated to the selected proteins (concentration of 2 mg/ml) using FluoroTag Kits (purchased from Molecular Probes) and according to the instructions of the manufacturer. The labelled proteins were separated from the unconjugated fluorescent dyes using a Sephadex G-25 column. The concentration of labelled proteins was determined by UV–vis spectroscopy (Varian). The fluorescent dye/protein molar ratio of the purified protein was determined by measuring the absorbance at 280 nm (for protein) and 556 nm (for AlexaFluor 546).

The fluorescently labelled proteins (10 μl of solutions with concentrations of 0.014, 0.07 and 0.14 mg/ml), diluted from stock solutions, were deposited on microstructured PMMA surfaces flooding the whole surface of the microassay. The slide was incubated for 30 min at room temperature in a humid chamber, and then washed three times with PBS and twice with Nanopure water. The same procedure was applied to the control surfaces, i.e., flat PMMA.

Fig. 1 presents a scheme of the process flow of the fabrication of protein arrays. Supplementary information (Fig. S1) presents typical fluorescent images of the protein microarrays and a typical atomic force microscopy scan of the microstructures.

2.3. Visualisation and quantification of the protein adsorption on microstructures

The attachment of fluorescently labelled proteins microstructured surfaces was visualised using two microscopes: a Nikon Microphot FX upright microscope with a UV light source (Nikon Mercury Lamp, HBO-100 W/2; Nikon C.SHG1 super high pressure mercury lamp power supply) at 100× objective, equipped with a Nikon camera (FX-35WA); and the Nikon inverted microscope on which the Laser Scissors System was mounted, i.e., a Nikon Eclipse TE-DH 100 W, 12 V, with a UV light source (Nikon TE-FM Epi-Fluorescence) and equipped with a Nikon Charged Coupling Device (CCD) camera. These systems have been used to capture both the bright field and fluorescent images of microfabricated structures with immobilised proteins. In order to obtain statistically meaningful transversal profiles of the fluorescence, the image was bit-mapped and the pixel intensities have been averaged along the axis of the microstructures.

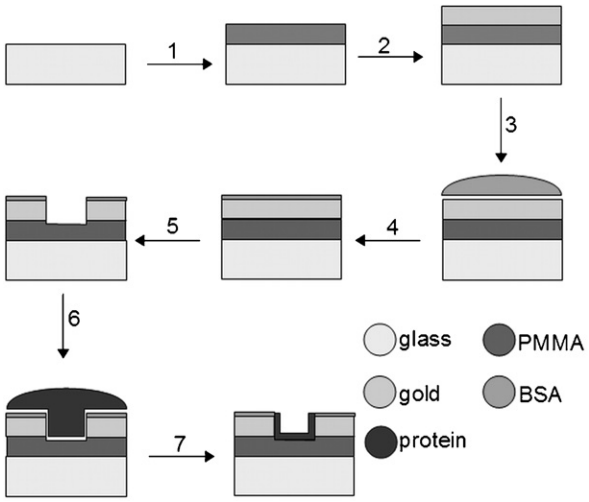

Fig. 1. Scheme of the process flow for the fabrication of protein arrays based on microablated surfaces.

The overall fluorescence intensities of the proteins immobilised on microstructures and on control flat surfaces have been quantified using a fluorimeter (FLUOStar Galaxy, from BMG Labtech, Germany) by measuring the emission at 556 nm with excitation at 583 nm. Calibration curves have been generated for each protein to factor in the degree of labelling. The overall fluorescence readout has been weighted using the ratio between the area of the microstructured surfaces on which the proteins are adsorbed and the total area (approx. 0.1 mm^2) of the deposited droplet of protein solution. For these quantification experiments it has been found that the optimum protein concentration in solution that ensures the accurate concentration-modulated fluorescent signal of the surface is 0.1 mg/ml, as also reported elsewhere for HSA (Sheller et al., 1998). The adsorption is reported in relative values, i.e., equivalent protein concentration in solution, expressed in mg/ml, representing a concentration in solution which would give the same level of fluorescence for the same droplet volume. The reported results are the mean values of nine repeats from three independent experiments.

2.4. Atomic force microscopy

Atomic force microscopy (AFM) was carried out on an Explorer system (ThermoMicroscopes) in the normal contact mode. The AFM system is based on the detection of tip-to-surface forces through monitoring optical deflection of a laser beam incident on a force-sensing/imposing lever. Several scanners were used in order to cover the scales of lateral topographical and chemical differentiation. The fields-of-view ranged from 100 μm × 100 μm down to 8 μm × 8 μm. The analyses were carried out under air-ambient conditions (temperature of 23 °C and 45% relative humidity). Pyramidal-tipped, silicon nitride cantilevers with a spring constant

Table 1
Molecular characteristics of the model proteins. The surface amphilicity of the proteins have been calculated by probing the surface with a sphere with 10 Å radius, which is similar with the roughness of the polymeric surfaces.

No	Protein (PDB ID)	MW (kDa)	Surface (Å^2)1.4 Å/(10 Å)	Residues (atoms)	IP (charge)	Bulk/(surface) amphilicity
1	Lysozyme (1lyz)	14.3	8446 (4212.7)	129 (993)	11 (−43.86)	0.55 (54)
2	Myoglobin (1mbn)	17.2	8059 (5228.3)	153 (1216)	7 (−31.76)	0.92 (25.64)
3	α-Chymotrypsin (2cha)	25.2	20969 (11648.3)	241 (3472)	9.1 (−97.91)	0.41 (74.9)
4	Human serum albumin (1ao6)	66.5	40051 (15663.3)	585 (4600)	4.7 (−236.08)	0.89 (92.24)
5	Human immunoglobulin (1igt)	145.3	83495 (40144.4)	1316 (10214)	6.55 (−443.32)	0.56 (157.4)

of 0.032 N/m were used. As the tip scans across the surface, the lateral force acting on the tip manifests itself through a torsional deformation of the lever, which is sensed by the difference signal on the Left–Right signal on the quadrant detector. The difference signal can be plotted as a function of x–y location in the topographical field of view, and the resulted friction force image can then be correlated directly with the topographical image.

To obtain statistically relevant transversal profiles of the topography and lateral force, the image was statistically processed using WSxM software (from Nanotec Electrónica).

2.5. Simulation of the microablation-induced evolution of temperature

The evolution of the temperature in the metal and polymeric film during and after ablation has been simulated solving a bi-dimensional heat conduction equation, which also takes into account the radiative transfer and the surface reflectivity, using a finite element commercial software, COMSOL Multiphysics. The laser data have been used as described above and the material parameters have been collected from the open literature. The simulated domain comprises a vertical rectangle of 10 μm wide × 50 nm deep area, representing the Au layer; on top of a rectangle of 10 μm × 500 nm, representing the PMMA layer. We used the thermal isolation as boundary conditions, except for the interface Au–air, where radiative and convective heat transfer condition was employed. A full account of the simulation assumptions, settings and results is provided in Supplementary information S2.

2.6. Protein molecular parameters

The molecular structures of the selected proteins have been imported from the Protein Data Bank (PDB) (Berman et al., 2000; Bernstein et al., 1977). The structure and the molecular surface of the selected proteins have been visualised using the freely available structure visualisation software ViewerLite (from Accelerys).

Several molecular descriptors of the selected proteins have been either collected from the literature (molecular weight, number of residues, isoelectric point); or calculated as follows.

First, the bulk properties, i.e., total charges and bulk hydrophobicity have been calculated using a simple routine reported before (Vasina et al., 2009), consisting in adding the hydrophobicities and charges of each residue and atom, respectively, present in the protein. The chosen hydrophobicity scale (ΔGoct, from White and Wimley, 1998) is physically representative as it reports the amino acid contribution to the free enthalpy of the transfer of a peptide passing through a water–octanol interface. The charges of individual atoms in amino acids have been calculated using a semi-empirical method (PM3 as implemented in HyperChem from HyperCube Inc.) at different pH; then averaged according to acid–base equilibria equations. This procedure allows the calculation of the charges as function of the pH of the solution.

Secondly, molecular surface properties, i.e., molecular surface and surface hydrophobicity, have been calculated using an upgraded version of a software program, which uses Connolly's algorithm (Connolly, 1993) for visualisation of molecular surfaces. Briefly, the upgraded program calculates the properties as encountered on the molecular surface by probing balls with different radii. The properties of the proteins have been calculated with the default probe radius, i.e., 1.4 Å.

The protein molecular parameters are presented in Table 1. A full account of the molecular parameters is presented in Supplementary information S3.

3. Results and discussion

3.1. Microablation-induced thermo-chemical processes in micro/nano-confined volume

Initial work regarding the proposed technology (Ivanova et al., 2002) indicated that the polymer beneath the metal layer is affected by microablation, usually resulting in a hole with elevated ridges at the edges of the microstructures. Recent experiments (Dobroiu et al., 2010) explored to a fuller extent the nanotopography of the microstructures modulated by ablation parameters, i.e., laser wavelengths and energies; and by material parameters, i.e., metal and polymeric films of various nature and thicknesses. The proposed methodology uses micro-scale fabrication, i.e., ablation with beams in the micron-range, to produce, by localised self-assembly following the reorganisation of material post-ablation, 100 nm-range structures.

It has been found that, depending on the combination experimental conditions, one can obtain three types of sub-micrometre profiles, i.e., domes, ripples and holes. These typical topographies appear to be the result of intense polymer pyrolysis at the interface with the ablatable metal layer. While the very small reaction volume, i.e., up to 5 μm laterally, and up to few hundred nm vertically, make the use of the usual analytical techniques inapplicable, three methodological tools are available to understand the outcome of the pyrolysis processes induced by laser microablation: (i) the simulation of the temperature evolution during and after microablation pulse; (ii) the comparison of the energies of reaction for different reaction pathways of PMMA pyrolysis; and, most importantly, (iii) the AFM measurements of the topographies and lateral force transversally to the microstructures.

Simulation of the microablation. The results of the simulation of the evolution of the temperature in the stacked metal–polymer layer during the ablation of the metal could be summarised as follows:

(i) Au melts during the ablation process and this molten state lasts approximately 50 ns, beyond the 4 ns of the laser pulse. During this period, a velocity field is created sideways in the melt. As a result the metal and the polymer, if melted, move aside from the centre of the ablated area.
(ii) The temperature does not reach the Au vaporisation temperature, even in the middle of the ablated area. Therefore the polymer beneath is exposed to a process of pyrolysis, lasting

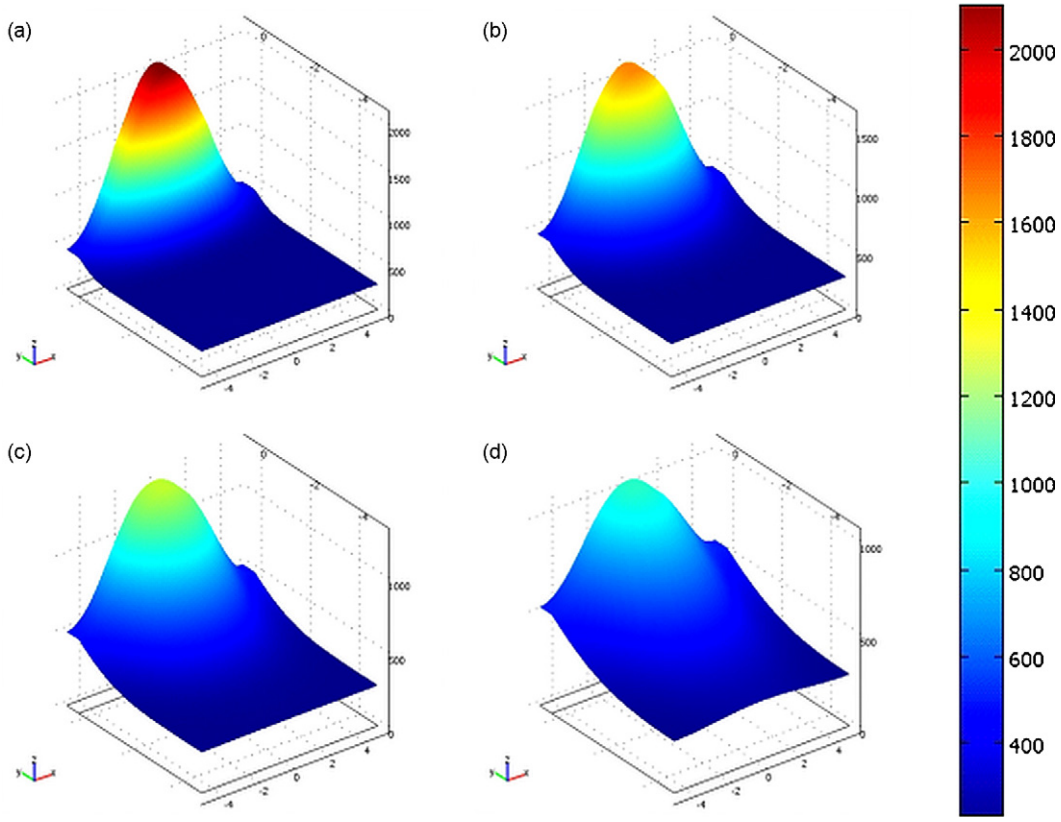

Fig. 2. Simulation results for the evolution of temperature. From left to right and top to bottom: profile of the temperature at 10, 25, 50 and 100 ns. While the vertical scale is normalised for each plot, the coloured scale is common to all graphs.

more than 50 ns, under a molten layer, which is effervescent and decreasing in thickness.

(iii) The variation and the evolution of the temperature during the ablation period (5 ns) and after (up to 100 ns), as synthetically presented in Fig. 2, is nearly fully confined laterally in the microablated area; and in the polymer layer down to approximately 200 nm, where it reaches 200 °C after 100 ns.

This exploratory simulation did not take into consideration the loss of material during ablation and the loss of heat due to endothermic pyrolysis process, which would require more advanced simulations (under development). However, as these two processes are thermally contradictory, i.e., the removal of material will translate to an advancement of the high temperature front; but will also remove heat from the system, we can assume that the simulated evolution of the temperature reflects well, in the first approximation, the reality of microablation process. It is also reasonable to expect that the processes in the polymer, discussed further, which produce a large volume of gaseous products, are likely to contribute to movement of mass sideways. Moreover, this movement will produce crater-like structures, which are generally encountered in microablation processes (Dahotre, 2007; Pereira et al., 2004; Sim and Kim, 2005; Vestentoft and Balling, 2006).

Enthalpies of pyrolysis reactions of PMMA. The examination of Table 2, which presents the enthalpies of reaction for different pyrolysis products of PMMA (calculated using quantum mechanics methods; edited from a recent contribution, Stoliarov et al., 2003), can be summarised as follows:

(i) The depolymerisation of PMMA. i.e., reaction 1a and 1b, is the most energetically favourable. These reaction routes will lead to lower molecular weight, but essentially chemically similar polymeric species.

(ii) The second most favourable pyrolysis process is the de-esterification of PMMA (reaction 2), which could lead to either poly(methyl acrylic acid) through the capturing of a H (reaction not shown), or to decarboxylation (reaction 5), the latter being an exothermic process leading to an aliphatic polymer (identical product with that from the reaction 3, having a higher enthalpy of reaction). Interestingly, depending on the path and advancement of reactions, i.e., [(2) + (5) and (3)] or [(2) + H capture], the resulting material will be very different, i.e., an aliphatic polymer, hydrophobic and with a low glass transition (T_g) polymer, hence soft; or an acrylic acid, which is hydrophilic and rigid (high T_g).

(iii) Finally, the reaction path 4 leads to an aldehyde, which should be mildly hydrophilic.

While all the above processes will occur in parallel in the micro/nanometer-scale furnace, which is confined between the ablating metal roof and polymer floor and walls, given this ladder of enthalpies of reaction and the decrease of the energy provided by the laser ablation from the centre of the nanostructure towards its edges, it is reasonable to expect that the following material composition exists on the micro/nanostructured surface:

(i) PMMA is likely to be present throughout the surface of microstructure, from the edges to the centre, at various concentrations and degrees of polymerisation. The depolymerisation, which should be the most intense in the middle of the microstructure, could lead to the formation of individual monomers, which are volatile or burnt, thus explaining in part the disappearance of the material.

Table 2
Enthalpies of reaction for several pyrolysis pathways of PMMA.

No.	Reaction	ΔH° (kJ/mol)
1a	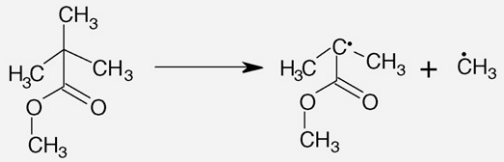	329
1b	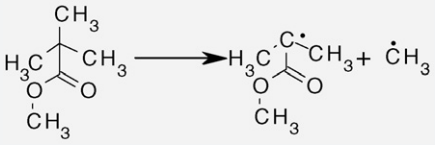	332
2	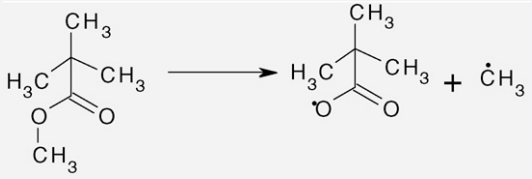	364
3	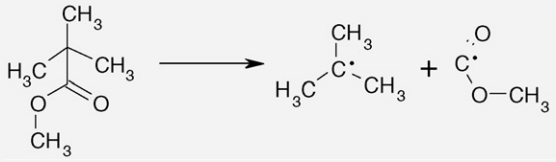	383
4	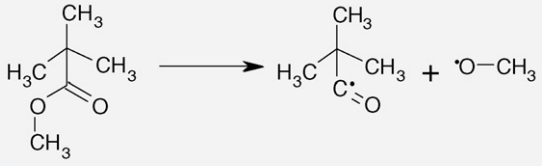	420
5	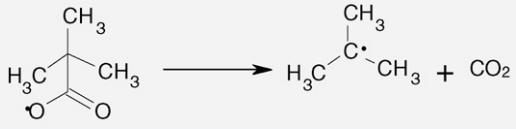	−72

(ii) Towards the edges of the microstructure the surface is more hydrophobic and mechanically soft, due to the aliphatic nature of the polymer, i.e., lacking any ester, aldehydic/ketonic, or acidic groups.
(iii) In the middle of the microstructure the surface is less hydrophobic and mechanically harder as the polymer contains acidic or aldehide groups.

These assumptions are further compared with AFM and protein adsorption data.

Analysis of AFM topographies and lateral force data. AFM has been used to probe intermolecular interactions with pN sensitivity and nm-spatial resolution more than a decade ago (Noy et al., 1997). When imaging under ambient conditions, the capillary condensation between the tip and sample surfaces reflects the relative degree of hydrophilicity and can be used as a basis for discriminating between hydrophobic and hydrophilic groups (Wilbur et al., 1995), thus the image contrast in a lateral force map is effectively a measure of tip-to-surface friction. Frictional force follows the generalised Amonton's law (Noy et al., 1997; Sinniah et al., 1996; Vezenov et al., 1997; Braun and Naumovets, 2006; Butt et al., 2005):

$$F_f = \mu F_N + F_0 \quad (1)$$

where μ is friction coefficient, F_N is the lever-induced normal force and F_0 is "residual force" which correlates with adhesion force between the tip and the sample surfaces.

Previous studies (Noy et al., 1997; and references therein) have shown that the interaction forces between tips and samples which both terminate with hydrophobic groups are small. Observed interaction forces are also small when one of the surfaces terminates with hydrophobic groups and the other terminates with polar groups, whereas significant interactions are observed when both the tip and sample surfaces terminate with hydrophilic groups (hydrogen-bonding). As the Si_3N_4 tip used in our study is hydrophilic due to the native oxide surface layer, the frictional force is therefore higher as the tip is scanned across a hydrophilic surface, compared to a hydrophobic surface (Burgos et al., 2007; Leggett et al., 2005).

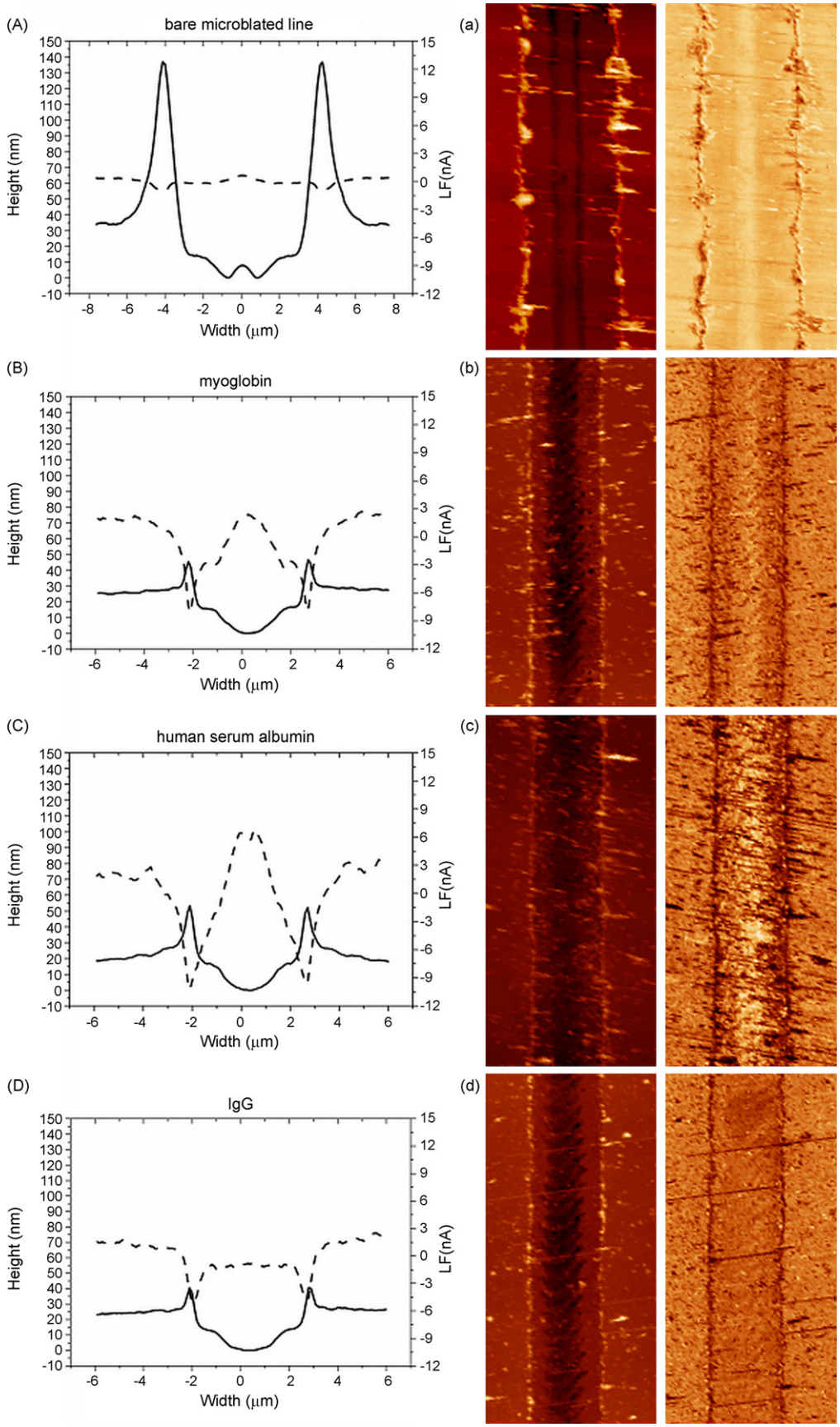

Fig. 3. AFM scans and analysis of the bare (top) and protein covered microstructures (myoglobin – second from the top; HSA – third from the top; and IgG – bottom). The images on the right represent the respective scans of topography (left) and lateral force (right). The plots on the left represent the averaged topographies (continuous line) and lateral force (dotted line) profiles.

While laser power does modulate the topography and physico-chemistry of the microstructured surface, the analysis of typical AFM scans, presented in Fig. 3, top row, indicate that, for the experimental conditions used here:

(i) The edges of the microstructures are elevated, depending on the laser power, at heights around 100 nm. This characteristic feature has been observed for other laser ablation induced micro/nanostructuring (Schwarz-Selinger et al., 2001; Dobroiu et al., 2010). The material in this area induces a slightly lower friction in the AFM tip than the rest of the material, possibly due to the aliphatic nature of the polymer, as described above. Also the soft mechanical nature of the polymer, due to the lower T_g of the polymer, or its porosity, dampens this hydrophobicity-induced lower friction.
(ii) At the centre of the microstructure, at the bottom of an approximately 50 nm deep well, the material induces a slightly higher friction of the AFM tip, possibly due to the less hydrophobic material. This effect could be also dampened by the higher polymer rigidity, which should be similar to that of the PMMA.

These findings validate both the temperature simulation results and also correlate well with the analysis of the enthalpies of reaction of PMMA pyrolysis.

3.2. Immobilisation of proteins on microstructures

Our initial study (Ivanova et al., 2002)presented the new technology for the fabrication of protein arrays comprising microstructures that encode microarray information; and demonstrated the operation, including the preservation of specific recognition, using model antibodies. During this study we noticed the lateral structuring of the distribution of protein concentration on microablated lines, but the imaging resolution was insufficient to analyse this behaviour in greater detail, either from the point of view of microstructure topography or the specific response of protein adsorption to diverse physico-chemistry presented on the surface. Subsequently, we explored the modulation of nanotopographies by laser and material parameters advancing the understanding of the processes responsible of these surface physico-chemistries (Dobroiu et al., 2010). In the previous sections of the present study we further clarified the nature and the geometrical distribution of the physico-chemistry for a special case – PMMA. Furthermore, we used two methodologies, i.e., florescence microscopy and quantification; and AFM mapping of topography and lateral force, to explore the interrelation between the protein parameters and local surface parameters in modulating the protein immobilisation on the chip surface.

Fluorescence imaging and quantification. As the immobilisation of diverse protein on the same microarray chip surface is a fundamental challenge, we studied the impact of the concentration of the protein in solution on the concentration of protein immobilised on the microstructures, as indicated by the respective fluorescence image. The result of this test is synthetically presented in Supplementary information (Fig. S4.1). It appears that IgG and, to a lesser extent, lysozyme produce strong fluorescent signals at even low concentrations in solution. At the other end of the spectrum, α-chymotrypsin and to a lesser extent human serum albumin produce low fluorescent signals for the tested concentration in solution. Although the contrast of the fluorescent images is low at submicron resolution, a representation of the fluorescent signal across the microstructure (Supplementary information Fig. S5.1) reveals a decrease of the lateral structuring of the protein concentration from myoglobin, to HSA and IgG.

A better quantification of the protein immobilisation on microstructures could be obtained by the comparison of the overall fluorescent signal on the microarray spot comprising the microstructures compared with a similar area of the bare polymer (PMMA); and by employing the extreme sensitivity of the photon counting system of the fluorimeter. For the optimal experimental conditions, i.e., moderate protein concentration in solution (0.1 mg/ml), it has been found that the adsorption of the proteins on microstructures increases, depending on the molecular weight or molecular surface of the respective protein, from 3- to 10-fold (Fig. 4).

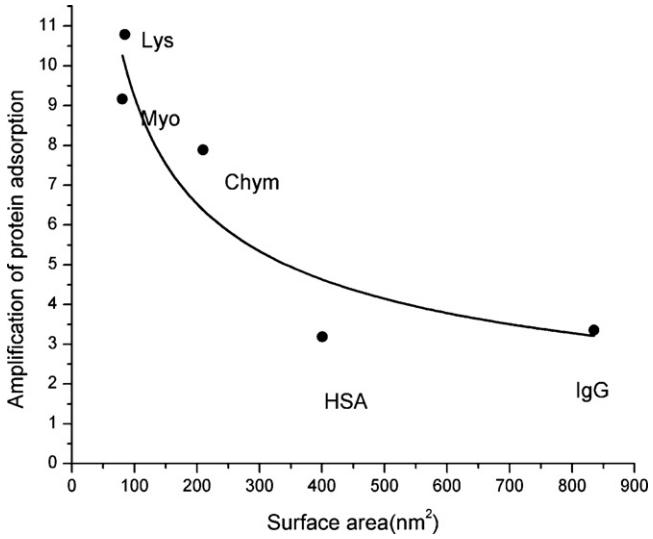

Fig. 4. Amplification of the protein adsorption vs. molecular surface (measured by the probing with a ball with 10 Å radius) of the respective proteins.

AFM measurements of topography and lateral force. The AFM analysis of the protein covered microstructures concentrated on three proteins, i.e., myoglobin (representing the small, globular proteins), HSA and IgG. The AFM imaging and analysis of the surface of the microstructures after protein immobilisation (Fig. 3) reveal two striking differences when comparing the bare surface comprising the microstructures surrounded by the BSA-coated surface with the surfaces exposed to protein solutions:

(i) Firstly, the elevated areas at the edges of the microstructures collapsed, decreasing from approximately 100 nm for the bare microstructured surfaces, to 20 nm for all samples presented to protein solutions, regardless of the protein used. This shrinkage can be explained by the relaxation of the polymer when exposed for 30 min to the aqueous protein-containing solution, possibly resulting in a more compact material. This polymer relaxation could also explain the disappearance of the fine structure in the middle of the microstructure, although the plateaus between the middle and the edges of the microstructure look more resilient to polymer relaxation.
(ii) Secondly, the lateral force encountered by the AFM tip at the edges of the microstructures present an important drop. In the present experimental context, this decrease in lateral force cannot be attributed to an increase in hydrophobicity, therefore this evolution can be explained only by the more compact nature of the polymer, as suggested above.
(iii) Thirdly, while the topography in the centre of the microstructure suffers only minor changes, the lateral force increases dramatically, bringing it close to or above the levels experienced by the AFM tip outside the microstructures, i.e., areas covered by BSA. This increase can be only explained by the consistently higher hydrophilic nature of the immobilised proteins. Similarly, it has been demonstrated before (Nicolau et al., 2005) that AFM lateral force imaging could distinguish

between surfaces that are covered by partially hydrophobic single stranded DNA from surfaces covered with comparatively more hydrophilic double-stranded DNA.

(iv) Furthermore, the lateral force profile presents a protein-specific structuring, with lateral terraces for myoglobin samples; a steep maximum for albumin samples with barely visible lateral shoulders; and a flat plateau for IgG. These profiles mirror approximately the transversal profiles of the florescent images of the protein covered microstructures.

3.3. Impact of molecular descriptors on protein adsorption on microstructures

Protein adsorption is critical for the performance of biomedical microdevices, comprising biosensors, lab-on-a-chip devices and microarrays, and particularly for the latter, which involve massive multiplexing. Indeed, the design, fabrication and operation of the protein chips are much more challenging than for their DNA counterparts, primarily because of two, inter-related surface-modulated processes: (i) the variations of the concentration of different proteins on the same chip surface, with impact on the readout, e.g., fluorescence intensity that are unrelated to bioactivity; and (ii) surface-induced protein denaturation, which also leads to erroneous readout, and certainly decrease of sensitivity (Huang, 2001; Templin et al., 2002). For protein arrays these problems are further exacerbated by the emergence of very large multiplexing micro and nano-arrays, where an additional challenge is to have similar concentrations and bioactivity of different proteins on the same chip surface, when surface-induced response varies importantly from protein to protein.

Along this line of reasoning, the cornerstone of the proposed protein microarrays technology is to fabricate and present to different protein surfaces with the expectation that this transformation from homogeneous combinatorial nature of the surface will allow different proteins to find the most suitable surface in terms of adsorption and preservation of bioactivity. While this surface-specific response will be also spatially addressable, because the different micro/nano-surfaces are co-located in a small area (around 10 μm or less channel width), the florescence signal will be recorded as being located in the same spot areas. Two important aspects remain to be analysed in the context of the modulation of immobilisation by protein parameters: the amplification of protein immobilisation on microstructures; and the specificity of protein immobilisation within the microstructures.

Amplification of protein immobilisation on microstructures. The amplification of the protein concentration on the surface, provided that the conformation does not change to an extent where the bioactivity would be severely affected, has been a methodology often used as means to boost the sensitivity of the biomedical microdevices. The simplest way to achieve this desideratum is by increasing the specific surface, e.g., surfaces with increased roughness, more porous surfaces, or nanostructured surfaces. In our experiments, the microablation increases the surface of the polymer in the ablated area of the channel, approximately by a factor of 3 (data not shown). While this amplification of the specific surface correlates well with the increase of the protein concentration for large proteins, i.e., HSA and IgG (far right in Fig. 4), the smaller proteins, such as lysozyme, myoglobin and α-chymotrypsin, present much higher amplification values.

Consequently, for these proteins, other more intricate mechanisms should be responsible for the amplification of adsorption. It has been demonstrated (Ostuni et al., 2003) that the proteins that are more hydrophobic will adsorb better and irreversibly on surfaces. In our study, the amplification of adsorption (presented in Fig. 4) increases with the increase of surface hydrophobicity (calculated on the molecular surface of the respective proteins, and presented in Table 1), but it is largely uncorrelated with the bulk hydrophobicity, which is a sum of the hydrophobicities of the residues of the respective protein. The surface hydrophobicity of the model proteins used in this study decreases with the molecular weight of the protein, with the exception of myoglobin, which is more hydrophobic than otherwise expected for its size. Indeed, small proteins are not able to protect well enough their hydrophobic core, thus leading to augmented amplification of adsorption. In this context, the specificity of myoglobin adsorption across the microablated channels (Fig. 3) could be understood as a specific response of the highest surface hydrophobicity of the tested proteins. Finally, the amplification of adsorption decreases with the increase of charging of specific protein, as charges are well inverse-correlated with hydrophobicity.

Given the above observations, we propose that the amplification of the protein adsorption of microstructured surfaces that present both higher specific surfaces (approximately 3-fold) and a combinatorial nature of their physico-chemistry, as compared with flat chemically homogeneous polymeric surfaces, can be explained as follows:

(i) Smaller proteins, which have reduced variation of the molecular surface, both in shape and chemistry, can capitalize better on the combinatorial nature of the microstructured surfaces, as they are more hydrophobic on their molecular surface.

(ii) Larger proteins, which have themselves a molecular surface with a combinatorial nature, are much more opportunistic and can adsorb on essentially any surface.

Specificity of protein immobilisation within the microstructures. The explanation proposed above is further validated by the analysis of the lateral force profiles of the protein covered microstructures. Indeed, a small protein, e.g., myoglobin, could differentiate between different surfaces co-located within the few microns-wide microstructured channels; a large protein, e.g., HSA, is far less specific; while a large and shape-complex protein, e.g., IgG, presents no specificity towards the adsorbing surface.

4. Conclusions

Polymer surfaces that have been exposed to a micro-confined pyrolysis induced by the microablation of a top metal layer exhibit 100 nm-range structures. These micro/nanostructured surfaces present a larger variability of topography and chemistry confined in a small, micro-sized area. Consequently, molecularly different proteins adsorbed at increased levels, between 3- to 10-fold compared to flat homogenous, chemically similar surfaces, and with propensity to counteract the surface-induced denaturation. Furthermore, fluorescence and AFM analysis demonstrated that smaller proteins with less diverse molecular surface can capitalize better on the combinatorial nature of the microstructured surfaces, while larger proteins, which have a molecular surface with a combinatorial nature themselves, are much more opportunistic and can adsorb on essentially any surface. These findings open new opportunities for both immediate applications, such as more sensitive protein arrays, and for fundamental studies regarding the interaction of proteins with nanostructures.

Acknowledgments

This study was supported by grants from the Defence Advanced Research Projects Agency (DARPA), Australian Research Council and by a European-Australia FP7 project (Bio-Inspired Self-assembled Nano-Enabled Surfaces – BISNES).

Contribution of the authors: DVN designed the experiments, analysed the measurements, wrote the paper and directed the research project; EPI designed the experiments, was responsible for protein-related work, data analysis and wrote the paper; FF simulated the process of microablation; LF, AV and YVA microfabricated the samples, immobilised the proteins and made the primary measurements; SD analysed the AFM data; and DKP run the AFM measurements.

Appendix A. Supplementary data

Supplementary data associated with this article can be found, in the online version, at doi:10.1016/j.bios.2010.07.044.

References

Berman, H.M., Westbrook, J., Feng, Z., Gilliland, G., Bhat, T.N., Weissig, H., Shindyalov, I.N., Bourne, P.E., 2000. The protein data bank. Nucleic Acids Res. 28 (1), 235–242.

Bernstein, F.C., Koetzle, T.F., Williams, G.J.B., Meyer, E.F., Brice, M.D., Rodgers, J.R., Kennard, O., Shimanouchi, T., Tasumi, M., 1977. Protein data bank—computer-based archival file for macromolecular structures. J. Mol. Biol. 112 (3), 535–542.

Braun, O.M., Naumovets, A.G., 2006. Nanotribology: microscopic mechanisms of friction. Surf. Sci. Rep. 60 (6–7), 79–158.

Burgos, P., Geoghegan, M., Leggett, G.J., 2007. Generation of molecular-scale compositional gradients in self-assembled monolayers. Nano Lett. 7 (12), 3747–3752.

Butt, H.J., Cappella, B., Kappl, M., 2005. Force measurements with the atomic force microscope: technique, interpretation and applications. Surf. Sci. Rep. 59 (1–6), 1–152.

Chovan, T., Guttman, A., 2002. Microfabricated devices in biotechnology and biochemical processing. Trends Biotechnol. 20 (3), 116–122.

Connolly, M.L., 1993. The molecular surface package. J. Mol. Graph. 11 (2), 139–143.

Dahotre, N.B., 2007. Laser Fabrication and Machining of Materials. Springer, New York.

Dobroiu, S., Delft, F.C.M.J.M.v., Thiel, E.v., Hanson, K.L., Nicolau, D.V., 2010. Laser-assisted structuring of metal–polymer bilayers for protein patterning. Microelectron. Eng. 87 (5–8), 1190–1194.

Hanson, K.L., Filipponi, L., Nicolau, D.V., 2005. Biomolecules and cells on surfaces—fundamental concepts. In: Muller, U.R., Nicolau, D.V. (Eds.), Microarray Technology and its Applications. Springer, Berlin, Heidelberg, pp. 23–44.

Hook, A.L., Anderson, D.G., Langer, R., Williams, P., Davies, M.C., Alexander, M.R., 2010. High-throughput methods applied in biomaterial development and discovery. Biomaterials 31 (2), 187–198.

Huang, R.P., 2001. Detection of multiple proteins in an antibody-based protein microarray system. J. Immunol. Methods 255 (1–2), 1–13.

Ivanova, E.P., Wright, J.P., Pham, D., Filipponi, L., Viezzoli, A., Nicolau, D.V., 2002. Polymer microstructures fabricated via laser ablation used for multianalyte protein microassay. Langmuir 18 (24), 9539–9546.

Leggett, G.J., Brewer, N.J., Chonga, K.S.L., 2005. Friction force microscopy: towards quantitative analysis of molecular organisation with nanometre spatial resolution. Phys. Chem. Chem. Phys. 7 (6), 1107–1120.

Nicolau, D.V., Pham, D.K., Ivanova, E.P., Wright, J.P., Lenigk, R., Smekal, T., Grodzinski, P., 2005. Tone reversal of an AFM lateral force image due to hybridization of oligonucleotides immobilised on polymers. Small 1 (6), 610–613.

Noy, A., Vezenov, D.V., Lieber, C.M., 1997. Chemical force microscopy. Annu. Rev. Mater. Sci. 27, 381–421.

Ostuni, E., Grzybowski, B.A., Mrksich, M., Roberts, C.S., Whitesides, G.M., 2003. Adsorption of proteins to hydrophobic sites on mixed self-assembled monolayers. Langmuir 19 (5), 1861–1872.

Pereira, A., Cros, A., Delaporte, P., Georgiou, S., Manousaki, A., Marine, W., Sentis, M., 2004. Surface nanostructuring of metals by laser irradiation: effects of pulse duration, wavelength and gas atmosphere. Appl. Phys. A: Mater. Sci. Process. 79 (4–6), 1433–1437.

Ray, S., Mehta, G., Srivastava, S., 2010. Label-free detection techniques for protein microarrays: prospects, merits and challenges. Proteomics 10 (4), 731–748.

Schwarz-Selinger, T., Cahill, D.G., Chen, S.C., Moon, S.J., Grigoropoulos, C.R., 2001. Micron-scale modifications of Si surface morphology by pulsed-laser texturing. Phys. Rev. B 64 (15), 155323.

Sheller, N.B., Petrash, S., Foster, M.D., Tsukruk, V.V., 1998. Atomic force microscopy and X-ray reflectivity studies of albumin adsorbed onto self-assembled monolayers of hexadecyltrichlorosilane. Langmuir 14 (16), 4535–4544.

Sim, B.C., Kim, W.S., 2005. Melting and dynamic-surface deformation in laser surface heating. Int. J. Heat Mass Transfer 48 (6), 1137–1144.

Steen, W.M., 1998. Laser Material Processing, second ed. Springer, London, New York.

Sinniah, S.K., Steel, A.B., Miller, C.J., ReuttRobey, J.E., 1996. Solvent exclusion and chemical contrast in scanning force microscopy. J. Am. Chem. Soc. 118 (37), 8925–8931.

Stoliarov, S.I., Westmoreland, P.R., Nyden, M.R., Forney, G.P., 2003. A reactive molecular dynamics model of thermal decomposition in polymers: 1. Poly(methyl methacrylate). Polymer 44 (3), 883–894.

Templin, M.F., Stoll, D., Schrenk, M., Traub, P.C., Vohringer, C.F., Joos, T.O., 2002. Protein microarray technology. Trends Biotechnol. 20 (4), 160–166.

Vasina, E.N., Paszek, E., Nicolau, D.V., Nicolau, D.V., 2009. The BAD project: data mining, database and prediction of protein adsorption on surfaces. Lab Chip 9 (7), 891–900.

Vestentoft, K., Balling, P., 2006. Formation of an extended nanostructured metal surface by ultra-short laser pulses: single-pulse ablation in the high-fluence limit. Appl. Phys. A: Mater. Sci. Process. 84 (1–2), 207–213.

Vezenov, D.V., Noy, A., Rozsnyai, L.F., Lieber, C.M., 1997. Force titrations and ionization state sensitive imaging of functional groups in aqueous solutions by chemical force microscopy. J. Am. Chem. Soc. 119 (8), 2006–2015.

White, S.H., Wimley, W.C., 1998. Hydrophobic interactions of peptides with membrane interfaces. Biochim. Biophys. Acta (BBA): Rev. Biomembr. 1376 (3), 339–352.

Wilbur, J.L., Biebuyck, H.A., Macdonald, J.C., Whitesides, G.M., 1995. Scanning force microscopies can image patterned self-assembled monolayers. Langmuir 11 (3), 825–831.